

Data-Driven Multi-Objective Controller Optimization for a Magnetically-Levitated Nanopositioning System

Xiaocong Li, *Member, IEEE*, Haiyue Zhu, *Member, IEEE*, Jun Ma, *Member, IEEE*, Tat Joo Teo, *Member, IEEE*, Chek Sing Teo, *Member, IEEE*, Masayoshi Tomizuka, *Life Fellow, IEEE*, and Tong Heng Lee

Abstract—The performance achieved with traditional model-based control system design approaches typically relies heavily upon accurate modeling of the motion dynamics. However, modeling the true dynamics of present-day increasingly complex systems can be an extremely challenging task; and the usually necessary practical approximations often renders the automation system to operate in a non-optimal condition. This problem can be greatly aggravated in the case of a multi-axis magnetically-levitated (maglev) nanopositioning system where the fully floating behavior and multi-axis coupling make extremely accurate identification of the motion dynamics largely impossible. On the other hand, in many related industrial automation applications, e.g., the scanning process with the maglev system, repetitive motions are involved which could generate a large amount of motion data under non-optimal conditions. These motion data essentially contain rich information; therefore, the possibility exists to develop an intelligent automation system to learn from these motion data, and to drive the system to operate towards optimality in a data-driven manner. Along this line then, this paper proposes a data-driven model-free controller optimization approach that learns from the past non-optimal motion data to iteratively improve the motion control performance. Specifically, a novel data-driven multi-objective optimization approach is proposed that is able to automatically estimate the gradient and Hessian purely based on the measured motion data; the multi-objective cost function is suitably designed to take into account both smooth and accurate trajectory tracking. In the work here, experiments are then conducted on the maglev nanopositioning system to demonstrate the effectiveness of the proposed method, and the results show rather clearly the practical appeal of our methodology for related complex robotic systems with no accurate model available.

Index Terms—Learning-based control, robot learning, data-driven optimization, iterative feedback tuning, magnetic levitation, robot control, precision motion control, nanopositioning.

I. INTRODUCTION

THE magnetically-levitated nanopositioning technique [1], [2] is a promising solution for ultra-clean or vacuum precision motion applications due to its excellent characteristics such as multi-axis mobility, ultra-precision, large motion

This work is supported by Collaborative Research Project U18-R-030SU under SIMTech-NUS Joint Lab on Precision Motion Systems (U12-R-024JL). (*Corresponding author: Haiyue Zhu.*)

X. Li, H. Zhu and C. S. Teo are with the Mechatronics Group, Singapore Institute of Manufacturing Technology, Singapore 138634. (e-mail: li_xiaocong@simtech.a-star.edu.sg, zhu_haiyue@simtech.a-star.edu.sg, csteo@simtech.a-star.edu.sg).

J. Ma and M. Tomizuka are with the Department of Mechanical Engineering, University of California, Berkeley, CA 94720, USA (e-mail: jun.ma@berkeley.edu, tomizuka@berkeley.edu).

T. J. Teo and T. H. Lee are with the Department of Electrical and Computer Engineering, National University of Singapore, Singapore 117583 (e-mail: eledttj@nus.edu.sg, eleleeth@nus.edu.sg).

stroke, contact- and dust-free usage, etc. However, due to its fully floating feature, the maglev nanopositioning system requires sophisticated motion control in all its six Degree-of-Freedom (DOF) to even simply stabilize at a constant position. The advanced multi-axis positioning and trajectory tracking further require high-performance precision motion control techniques [3]–[7] to reject the internal/external disturbances and eliminate the coupling effects between axes. Traditionally, such precision motion control systems are designed and optimized based on the model (when available) obtained from the first principle or system identification, i.e., model-based approach [8]–[11]. However, obtaining an accurate model for the multi-axis maglev nanopositioning system is challenging and time-consuming; and the model obtained is typically often not adequately representative of the true dynamics, e.g., the coupling between axes is often not taken into account. To address this often-occurring general issue, it is a notable trend where learning-based methods are increasingly being explored in literature, wherein model parameters are not precisely known, and yet the appropriately optimal control performance can be obtained [12]–[14]. This data-driven methodology enables learning from available signals in the past, and also prevailing, non-optimal control settings to achieve a significant performance improvement for various cases of real-world mechatronic systems [15]–[18].

Data-driven controls are essentially developed based on the concept that machines can improve their performance by learning from previous executions of the same or similar tasks, in a way that closely resembles how humans learn. A promising trend in data-driven controls is deep reinforcement learning [19], wherein a neural network policy is trained based on real-world motion data as well as appropriate simulations. In addition to this end-to-end approach, deep neural networks can also be used for trajectory tracking in many robotic applications [20]. However, the limitation of these neural network based approaches is the requirement for a massive amount of training data. Also, the uncertainty in the important system stability issue due to the black-box nature of neural networks often becomes a concern, especially for safety-critical applications. Apart from the neural network based approaches, [21] proposed a novel model-less feedback control design for soft robotics, and it was further extended to the hybrid position/force control problem in [22]. The proposed approaches in these works allow the manipulators to interact with several constrained environments safely and stably, and then generate a model-less feedback control policy from these interactions. It is worthwhile to note that these works are mainly focused on kinematic-model-free control instead of

dynamic-model-free control, i.e., the Jacobian is unknown and empirically estimated; therefore, challenges in dynamic control remain.

It is worthwhile to note that many industrial processes such as scanning, pick-and-place, welding, and assembly, involve repetitive motions; therefore, less computationally expensive learning approaches can be pursued. For instance, the Iterative Learning Control (ILC) is a data-driven method that is used widely in precision machines [23], [24] and robotics [25]–[28]. It makes use of the repetitive tracking error data gathered in previous cycles to improve the performance of the system in subsequent cycles in a feedforward manner. Thus, it is essentially a feedforward learning approach rather than feedback learning; nevertheless it can serve as a very useful complement to an existing feedback controller. In [29], the authors proposed a novel Gaussian process based feedback controller optimization algorithm with applications to quadrotors. This approach models the cost function as a Gaussian process and explores the new controller parameters with a safe performance guarantee. This enables automatic and safe optimization in repetitive robotic tasks without human intervention. However, while greatly effective especially in guaranteeing safety, the convergence is relatively slow as it takes about 30 iterations to converge.

The Iterative Feedback Tuning (IFT) methodology is one of the approaches in the class of fast-converging data-driven controller optimization algorithms [30]. Conceptually similar to the other approaches, it makes use of the actual motion data to estimate the cost function gradient without relying on the system model. In addition, the Hessian of the cost function can be estimated to speed up the convergence. The estimated gradient and Hessian are subsequently used in the Gauss-Newton optimization procedure to iteratively obtain the optimal controller parameters. This IFT approach has been widely used in many applications such as path-tracking control of industrial robots [17], [31], ultra-precision wafer stage [32], [33], flow control over a circular cylinder [34] and compliant rehabilitation robots [18], etc. Extensions of the IFT idea to other types of controller includes iterative dynamic decoupling control [35], disturbance observer sensitivity shaping [36], iterative feedforward tuning [37], [38], and 3-DOF controller tuning [39], [40] etc. However, most of the existing work focused mainly on accurate tracking and did not take smooth tracking into account. In fact, in semiconductor manufacturing and many other robotic applications, both accurate and smooth trajectory tracking are required [41], [42], and this challenge remains unsolved. Hence, the contribution of this paper is to propose a learning-based controller optimization algorithm to enable smooth and accurate tracking in repetitive tasks as illustrated schematically and conceptually in Fig. 1. To the best of our knowledge, this work is the first feedback controller optimization method to take into account both accurate and smooth tracking in a data-driven manner. Furthermore, it is worthwhile to note that the optimization process is both data-efficient and fast-converging.

This paper is organized as follows. In Section II, a brief description of the magnetically-levitated nanopositioning system is provided. Then, in Section III, the proposed multi-objective

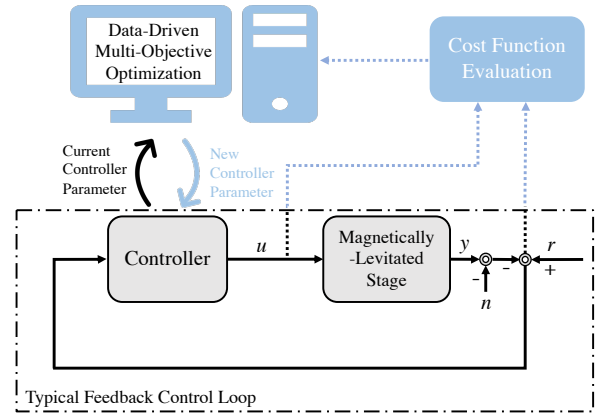


Fig. 1. Overview of the data-driven multi-objective controller optimization algorithm. The algorithm iteratively updates the controller parameters based on the actual motion data from the previous iteration to minimize the cost function value in an iterative and model-free manner.

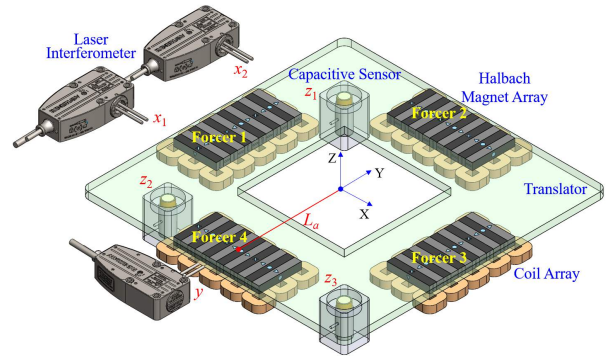


Fig. 2. Schematics of the square-coil-based magnetically-levitated planar nanopositioning system.

controller optimization algorithm is described and analyzed in detail. In Section IV, experimental work is conducted based on the magnetically-levitated nanopositioning system to show the effectiveness of the proposed algorithm. Finally, conclusions are drawn in Section V.

II. MAGNETICALLY-LEVITATED NANOPositionING SYSTEM

In this section, the magnetically-levitated planar nanopositioning system (which is the typical prototype application of our data-driven controller optimization approach) is first illustrated, including its working principles and associated overall control scheme. The design objective of our magnetically-levitated planar nanopositioning system is to enable 6-DOF motion with low system complexity and high energy efficiency. For large-stroke applications, the stroke expandability is also important as well as the affordability to simultaneously operate multiple motion translators. The schematic design of the implemented magnetically-levitated planar nanopositioning system for this work is illustrated in Fig. 2. Although the square coil array in Fig. 2 is covered here in a small area for evaluation, such a square coil based design allows suitably unlimited planar motion stroke as long as the coils spread

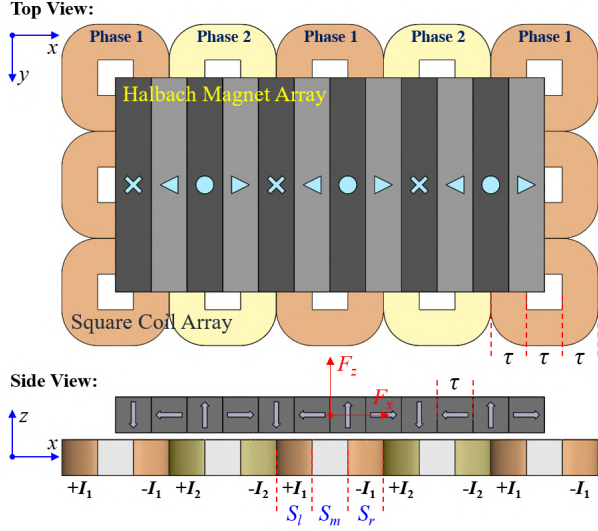


Fig. 3. Top view and side view of theforcer in the square-coil-based magnetically-levitated stage design.

over. Notably, this system adopts the tiled square coil array for actuation, which shows the comparative advantages in control complexity and energy efficiency as it only requires 8-phase for 6-DOF motion control and coils far away can be actively switched off to save energy [43]. Furthermore, the interference between coils is minimized at the maximum extent by using the square coil arrangement, so that multiple translators are feasible by individually controlling each or set of coils.

From Fig. 2, it can be seen that the 6-DOF motion is achieved by the combined force from Forcer 1 to 4, where each forcer can provide a vertical levitation force and horizontal thrust force. As illustrated in Fig. 3, the moving part of one forcer is a Halbach permanent magnet array and the stationary part is a square coil array grouped into two phases. Due to the periodic arrangement of magnetization directions indicated in Fig. 3, the Halbach array generates an almost ideal sinusoidal magnetic field in both X and Z axes except the magnet end effects. This is not achievable with the normal magnet array widely adopted in 1-DOF linear motors [43]. From the side view of Fig. 3, each square coil is divided into three segments, i.e., S_l , S_m , and S_r . The current directions in S_l and S_r are opposite and the magnetic field directions for S_l and S_r are also opposite, so that S_l and S_r generate identical force in both X and Z axes. S_m contributes zero force in two axes due to its current direction.

The force generation on a single square coil can be expressed via the relative location between coil and magnet arrays (x, z) as $F_x^c(x, z) = K_x(x, z)I$ and $F_z^c(x, z) = K_z(x, z)I$, where I is the current magnitude, and $K_x(x, z)$ and $K_z(x, z)$ are defined as,

$$\begin{aligned} K_x(x, z) &= C_f e^{-\gamma z} \left(-\sqrt{2}\tau \sin(\gamma x) + \frac{2\alpha}{\gamma} \sin(\gamma x) \cos\left(\frac{\gamma\tau}{2} + \beta\right) \right), \\ K_z(x, z) &= C_f e^{-\gamma z} \left(-\sqrt{2}\tau \cos(\gamma x) + \frac{2\alpha}{\gamma} \cos(\gamma x) \cos\left(\frac{\gamma\tau}{2} + \beta\right) \right), \end{aligned} \quad (1)$$

where $C_f > 0$ is a force constant, τ is the geometrical

dimension as indicated in Fig. 3, γ is the spatial wave number with $\gamma = \pi/2\tau$, and α and β are two constants numerically identified, $\alpha = 1.144$ and $\beta = 2.3924$. Therefore, the total force generated by the whole forcer in Fig. 3 is expressed via two phases of current as,

$$\mathbf{F}^f(x, z) = N \begin{bmatrix} K_x(x, z) & K_x(x + 3\tau, z) \\ K_z(x, z) & K_z(x + 3\tau, z) \end{bmatrix} \mathbf{I} \quad (2)$$

where $\mathbf{F}^f(x, z) = [F_x^f(x, z) \ F_z^f(x, z)]^T$, $\mathbf{I} = [I_1 \ I_2]^T$, I_1 and I_2 denote the current magnitudes in Phase 1 and Phase 2, respectively. N is the number of effective coils in each phase, where $N = 4$ for the case in Fig. 3, and denotes

$$\Phi_{\mathbf{K}}(x, z) = \begin{bmatrix} K_x(x, z) & K_x(x + 3\tau, z) \\ K_z(x, z) & K_z(x + 3\tau, z) \end{bmatrix}. \quad (3)$$

In order to control the 6-DOF motion, the global force/torque given by the controller needs to be allocated to four forcers. For each forcer, such local force is generated through energizing the two-phase current $\mathbf{I}_i = [I_{i1} \ I_{i2}]^T$ on each forcer. According to (2),

$$\mathbf{I}_i = \Phi_{\mathbf{K}}(x, z)^{-1} \mathbf{F}^{f_i} / N. \quad (4)$$

Therefore, the controllability of the square coil magnetically-levitated system design is based on the invertibility of $\Phi_{\mathbf{K}}(x, z)$. It is noted that

$$\begin{aligned} \det(\Phi_{\mathbf{K}}(x, z)) &= K_x(x, z)K_z(x + 3\tau, z) - K_z(x, z)K_x(x + 3\tau, z) \\ &= (C_f e^{-\gamma z})^2 \left(\left(-\sqrt{2}\tau \sin(\gamma x) + \frac{2\alpha}{\gamma} \sin(\gamma x) \cos\left(\frac{\gamma\tau}{2} + \beta\right) \right)^2 \right. \\ &\quad \left. + \left(-\sqrt{2}\tau \cos(\gamma x) + \frac{2\alpha}{\gamma} \cos(\gamma x) \cos\left(\frac{\gamma\tau}{2} + \beta\right) \right)^2 \right) \\ &= (C_f e^{-\gamma z})^2 \left(\sqrt{2}\tau - \frac{2\alpha}{\gamma} \cos\left(\frac{\gamma\tau}{2} + \beta\right) \right)^2. \end{aligned} \quad (5)$$

Since $\gamma = \pi/2\tau$, and thus $\gamma\tau = \pi/2$, it can be seen that as long as $\cos(\beta + \pi/4) \neq \sqrt{2}\pi/4\alpha$, $\det(\Phi_{\mathbf{K}}(x, z)) > 0$ indicates that $\Phi_{\mathbf{K}}(x, z)$ is full rank and invertible, with the values of the position (x, z) not affecting this property. Numerically, as the values of α and β are known, it is thus direct to verify that the condition $\cos(\beta + \pi/4) \neq \sqrt{2}\pi/4\alpha$ is met, which shows that (4) has no singularity and the 6-DOF motion is fully controllable. The 6-DOF sensing is achieved via three channels of laser interferometers (x_1, x_2, y) and three channels of capacitive sensors (z_1, z_2, z_3) as indicated in Fig. 2. With the measured 6-axis state-variables, each DOF can thus be closed-loop controlled as Single-Input Single-Output (SISO) systems and ready for the deployment of the algorithm in Section III.

III. DATA-DRIVEN MULTI-OBJECTIVE OPTIMIZATION

As noted earlier, certain important precision motion systems such as the maglev nanopositioning system emphasize the requirement for smooth and accurate tracking in terms of control performance. To achieve these objectives, both the

tracking accuracy and control signal variation needs to be taken into account concurrently in the optimization. Hence, the overall cost function in this paper is defined as

$$J(\mathbf{i}\rho) = \underbrace{w_1 e(\mathbf{i}\rho)^T \cdot e(\mathbf{i}\rho)}_{J_e} + \underbrace{w_2 \dot{u}(\mathbf{i}\rho)^T \cdot \dot{u}(\mathbf{i}\rho)}_{J_{\dot{u}}}, \quad (6)$$

where $\mathbf{i}\rho$ is the controller parameter vector in the \mathbf{i}^{th} iteration, and $J(\mathbf{i}\rho)$ is the total cost function consisting of the tracking related cost function J_e and control variation related cost function $J_{\dot{u}}$. Here, w_1 is the weighting for the tracking performance wherein $e(\mathbf{i}\rho)$ is the tracking error measured in the \mathbf{i}^{th} iteration; w_2 is the weighting for the control variation wherein $u(\mathbf{i}\rho)$ is the control input and $\dot{u}(\mathbf{i}\rho)$ is the variation of control input. Thus consider the typical feedback control system for the magnetically-levitated system as in Fig. 1, where a fixed structure controller $C(s)$ is used for motion control and can be expressed as

$$C(s, \rho) = \rho^T \bar{C}(s). \quad (7)$$

Here, ρ is a vector of the controller parameters to be optimized and $\bar{C}(s)$ is a vector of parameter independent transfer functions. We can now formulate the data-driven multi-objective optimization problem as:

Problem 1. Assume the motion system is unknown and controlled by a fixed structure controller $C(s, \rho)$ in (7); use only the closed-loop experimental data to determine the parameter vector ρ that minimizes the multi-objective cost function $J(\rho)$ (6), i.e., to find

$$\rho^* = \arg \min_{\rho} J(\rho). \quad (8)$$

A. Gradient Calculation and Estimation

With equation (6), the gradient of the cost function $J(\mathbf{i}\rho)$ with respect to the parameter in the \mathbf{i}^{th} iteration $\mathbf{i}\rho$ can be derived as

$$\begin{aligned} \nabla J(\mathbf{i}\rho) &= 2w_1 [\nabla \mathbf{i}e(\mathbf{i}\rho)]^T \cdot \mathbf{i}e(\mathbf{i}\rho) \\ &\quad + 2w_2 [\nabla \mathbf{i}\dot{u}(\mathbf{i}\rho)]^T \cdot \mathbf{i}\dot{u}(\mathbf{i}\rho), \end{aligned} \quad (9)$$

and the Hessian of the cost function can be approximated as

$$\begin{aligned} \nabla^2 J(\mathbf{i}\rho) &= 2w_1 [\nabla \mathbf{i}e(\mathbf{i}\rho)]^T \cdot \nabla \mathbf{i}e(\mathbf{i}\rho) \\ &\quad + 2w_2 [\nabla \mathbf{i}\dot{u}(\mathbf{i}\rho)]^T \cdot \nabla \mathbf{i}\dot{u}(\mathbf{i}\rho). \end{aligned} \quad (10)$$

The purpose of obtaining the gradient and the Hessian of the cost function is to apply the Newton's optimization algorithm [44]:

$$\mathbf{i}^{+1}\rho = \mathbf{i}\rho - \mathbf{i}\gamma (\nabla^2 J(\mathbf{i}\rho))^{-1} \nabla J(\mathbf{i}\rho). \quad (11)$$

where $\mathbf{i}^{+1}\rho$ is the updated parameter value for iteration $\mathbf{i} + 1$ and $\mathbf{i}\gamma$ is the step size at iteration \mathbf{i} . From (9) and (10), the Newton's optimization algorithm requires $\nabla \mathbf{i}e(\mathbf{i}\rho)$, $\nabla \mathbf{i}\dot{u}(\mathbf{i}\rho)$, $\mathbf{i}e(\mathbf{i}\rho)$ and $\mathbf{i}\dot{u}(\mathbf{i}\rho)$. $\mathbf{i}e(\mathbf{i}\rho)$ and $\mathbf{i}\dot{u}(\mathbf{i}\rho)$ can be obtained directly from the sensor measurement and the control software. However, $\nabla \mathbf{i}e(\mathbf{i}\rho)$ and $\nabla \mathbf{i}\dot{u}(\mathbf{i}\rho)$ cannot be obtained directly and have to be estimated with the input-output data collected from

the closed-loop experiments. The gradient of the tracking error can be derived as:

$$\nabla \mathbf{i}e(\mathbf{i}\rho) = \frac{-P \frac{\partial C(\mathbf{i}\rho)}{\partial \mathbf{i}\rho}}{[1 + PC(\mathbf{i}\rho)]^2} \cdot r = -\frac{P \frac{\partial C(\mathbf{i}\rho)}{\partial \mathbf{i}\rho}}{1 + PC(\mathbf{i}\rho)} \cdot \mathbf{i}e(\mathbf{i}\rho).$$

Inspired by the IFT approach [30], $\nabla \mathbf{i}e(\mathbf{i}\rho)$ can then be obtained by setting $\mathbf{i}e(\mathbf{i}\rho)$ as the new reference r in the "special" experiment, and we have

$$\nabla \mathbf{i}e(\mathbf{i}\rho) = -\frac{\partial C(\mathbf{i}\rho)}{\partial \mathbf{i}\rho} \cdot \frac{1}{C(\mathbf{i}\rho)} \cdot y_s, \quad (12)$$

where y_s denotes the position measurement for this experiment. Apart from $\nabla \mathbf{i}e(\mathbf{i}\rho)$, the gradient of $\mathbf{i}\dot{u}(\mathbf{i}\rho)$ can also be derived as

$$\begin{aligned} \nabla \mathbf{i}\dot{u}(\mathbf{i}\rho) &= \frac{\frac{\partial C(\mathbf{i}\rho)}{\partial \mathbf{i}\rho} [1 + PC(\mathbf{i}\rho)]}{[1 + PC(\mathbf{i}\rho)]^2} \cdot \dot{r} - \frac{P \frac{\partial C(\mathbf{i}\rho)}{\partial \mathbf{i}\rho} C(\mathbf{i}\rho)}{[1 + PC(\mathbf{i}\rho)]^2} \cdot \dot{r} \\ &= \frac{\partial C(\mathbf{i}\rho)}{\partial \mathbf{i}\rho} \frac{1}{1 + PC(\mathbf{i}\rho)} \cdot \dot{e} \end{aligned} \quad (13)$$

$\nabla \mathbf{i}\dot{u}(\mathbf{i}\rho)$ can be estimated with the same special experiment by feeding in $\mathbf{i}e(\mathbf{i}\rho)$ as the reference r

$$\nabla \mathbf{i}\dot{u}(\mathbf{i}\rho) = \frac{\partial C(\mathbf{i}\rho)}{\partial \mathbf{i}\rho} \cdot \frac{1}{C(\mathbf{i}\rho)} \cdot \dot{u}_s, \quad (14)$$

where u_s denotes the control input of this special experiment. Notice that $\nabla \mathbf{i}e(\mathbf{i}\rho)$ and $\nabla \mathbf{i}\dot{u}(\mathbf{i}\rho)$ can be estimated solely based on the experimental data. In addition, $\mathbf{i}e(\mathbf{i}\rho)$ and $\mathbf{i}\dot{u}(\mathbf{i}\rho)$ can be directly obtained or calculated based on the sensor measurement and control software. Hence, the gradient $\nabla J(\mathbf{i}\rho)$ and Hessian $\nabla^2 J(\mathbf{i}\rho)$ of the cost function can also be estimated according to (9) and (10). It should be noted, as will be discussed in Section III-B and III-C, that an additional normal experiment needs to be conducted in order to obtain an unbiased estimate of the gradient when the measurement noise is taken into consideration.

B. Data Collection

To make the data-driven optimization procedure clearer, all the experiments needed and data to be collected within a single iteration are listed below.

- Experiment I: Normal experiment.

$$r^1 = r, \quad (15)$$

$$y^1 = \frac{PC(\mathbf{i}\rho)}{1+PC(\mathbf{i}\rho)} \cdot r^1 - \frac{1}{1+PC(\mathbf{i}\rho)} \cdot n^1, \quad (16)$$

$$e^1 = \frac{1}{1+PC(\mathbf{i}\rho)} \cdot r^1 + \frac{1}{1+PC(\mathbf{i}\rho)} \cdot n^1. \quad (17)$$

- Experiment II: Special experiment.

$$r^2 = e^1, \quad (18)$$

$$y_s = y^2 = \frac{PC(\mathbf{i}\rho)}{1+PC(\mathbf{i}\rho)} \cdot e^1 - \frac{1}{1+PC(\mathbf{i}\rho)} \cdot n^2, \quad (19)$$

$$u_s = u^2 = \frac{C(\mathbf{i}\rho)}{1+PC(\mathbf{i}\rho)} \cdot e^1 + \frac{C(\mathbf{i}\rho)}{1+PC(\mathbf{i}\rho)} \cdot n^2. \quad (20)$$

- Experiment III: Normal experiment.

$$r^3 = r, \quad (21)$$

$$e^3 = \frac{1}{1+PC(\mathbf{i}\rho)} \cdot r^3 + \frac{1}{1+PC(\mathbf{i}\rho)} \cdot n^3. \quad (22)$$

$$u^3 = \frac{C(\mathbf{i}\rho)}{1+PC(\mathbf{i}\rho)} \cdot r^3 + \frac{C(\mathbf{i}\rho)}{1+PC(\mathbf{i}\rho)} \cdot n^3. \quad (23)$$

The bold right superscript refers to the experiment index within a single iteration. In Experiment I, the normal operation with, e.g., a S-curve trajectory, is conducted while y^1 is measured and used to generate e^1 as the reference of Experiment II. In Experiment II, measurement of y_s and u_s is taken and it is then used to obtain $\nabla^i e^i(\rho)$ and $\nabla^i \dot{u}^i(\rho)$ according to (12) and (14). In Experiment III, measurement of e^3 and u^3 is taken and used to calculate the cost function gradient $\nabla J^i(\rho)$. The complete data-driven multi-objective optimization algorithm can be summarized in **Algorithm 1**. It is worth noting that, similar to the IFT and many other algorithms inspired by the IFT, there is no strong guarantee (proofs) for robust stability throughout the iterations, due to the lack of the system model. Hence, as also suggested in [45], we shall use cautious updates, i.e., use small step-sizes, especially during the first iterations.

Algorithm 1 Data-Driven Multi-Objective Controller Optimization Algorithm

- 1) Set the iteration number $\mathbf{i} = 0$ and select the initial controller parameter ${}^0\rho$.
 - 2) Conduct Experiment I and measure the output y^1 and tracking error e^1 .
 - 3) Evaluate the cost function $J^i(\rho)$. Stop if the cost function value is satisfactory. Otherwise, proceed to Step 4.
 - 4) Conduct Experiment II and measure the output y^2 from this special experiment.
 - 5) Obtain $\nabla^i e^i(\rho)$ and $\nabla^i \dot{u}^i(\rho)$ according to (12) and (14) respectively.
 - 6) Conduct Experiment III and measure e^3 and u^3 .
 - 7) Compute $\nabla J^i(\rho)$ as well as $\nabla^2 J^i(\rho)$ according to (9) and (10), where ${}^i e^i(\rho)$, ${}^i \dot{u}^i(\rho)$ are obtained from Experiment III and $\nabla^i e^i(\rho)$, $\nabla^i \dot{u}^i(\rho)$ are obtained from Step 5.
 - 8) Execute the Gauss-Newton algorithm (11), and update the controller parameters.
 - 9) Set the iteration number $\mathbf{i} \leftarrow \mathbf{i} + 1$ and proceed to Step 2.
-

C. Unbiasedness of the Gradient Estimation

The cost function gradient is estimated using the closed-loop experiment data, so the measurement noises can potentially lead to errors during this estimation. For this stochastic approximation method to work, the gradient estimation has to be unbiased, mathematically

$$E\{\text{est}[\nabla J^i(\rho)]\} = \nabla J^i(\rho). \quad (24)$$

To prove the unbiasedness, we have the following assumptions:

Assumption 1. *Noises n in different experiments are independent from each other.*

Assumption 2. *Noises n are zero mean, weakly stationary random variables.*

Theorem 1. *For the motion system under the feedback control configuration as shown in Fig. 1, with Assumption 1 and Assumption 2, the estimation of the gradient of the cost function J in (6) is unbiased.*

Proof. From (12), the estimated gradient of e is given by

$$\begin{aligned} \text{est}[\nabla^i e^i(\rho)] &= -\frac{\partial C^i(\rho)}{\partial^i \rho} \cdot \frac{P}{1 + PC^i(\rho)} \cdot e^1 \\ &\quad - \frac{\partial C^i(\rho)}{\partial^i \rho} \cdot \frac{P}{[1 + PC^i(\rho)]^2} \cdot n^1 \\ &\quad + \frac{\partial C^i(\rho)}{\partial^i \rho} \cdot \frac{1}{C^i(\rho)} \cdot \frac{1}{1 + PC^i(\rho)} \cdot n^2 \\ &= \nabla^i e^i(\rho) + w_e, \end{aligned} \quad (25)$$

where

$$\begin{aligned} w_e &\equiv -\frac{\partial C^i(\rho)}{\partial^i \rho} \cdot \frac{P}{[1 + PC^i(\rho)]^2} \cdot n^1 \\ &\quad + \frac{\partial C^i(\rho)}{\partial^i \rho} \cdot \frac{1}{C^i(\rho)} \cdot \frac{1}{1 + PC^i(\rho)} \cdot n^2. \end{aligned} \quad (26)$$

Notice that w_e contains noises from Experiment I and Experiment II and e^3 contains only the noises from Experiment III. With Assumption 1 and Assumption 2, we have

$$E[w_e^T \cdot e^3(\rho)] = E[w_e^T] \cdot E[e^3(\rho)], \quad (27)$$

and

$$E[w_e^T] = 0. \quad (28)$$

Similar results can be obtained for \dot{u} from (14). The expectation of the estimation of the cost function gradient can be derived as follows

$$\begin{aligned} E\{\text{est}[\nabla J^i(\rho)]\} &= 2w_1 E\{\text{est}[\nabla e^T(\rho)]e^3(\rho)\} \\ &\quad + 2w_2 E\{\text{est}[\nabla \dot{u}^T(\rho)]\dot{u}^3(\rho)\} \\ &= 2w_1 E[\nabla e^T(\rho)e^3(\rho)] + 2w_1 E[w_e^T \cdot e^3(\rho)] \\ &\quad + 2w_2 E[\nabla \dot{u}^T(\rho)\dot{u}^3(\rho)] + 2w_2 E[w_{\dot{u}}^T \cdot \dot{u}^3(\rho)] \\ &= \nabla J^i(\rho) + 0 \cdot E[e^3(\rho)] + 0 \cdot E[\dot{u}^3(\rho)] \\ &= \nabla J^i(\rho). \end{aligned} \quad (29)$$

This completes the proof of the Theorem. \square

From the proof, it can be noticed that Experiment III is indeed necessary in order to guarantee the unbiasedness of cost function gradient estimation. If the data from Experiment I were used, i.e., $e^1(\rho)$ and $\dot{u}^1(\rho)$ instead of $e^3(\rho)$ and $\dot{u}^3(\rho)$, the same noise would exist in both $\text{est}[\nabla e^T(\rho)]$ and $e^1(\rho)$ (as well as in $\text{est}[\nabla \dot{u}^T(\rho)]$ and $\dot{u}^1(\rho)$). This would lead to a biased estimation for the cost function gradient and it is exactly the reason why Experiment III is needed.

IV. EXPERIMENTAL VALIDATION

This section documents the experimental results of using the proposed data-driven optimization algorithm for the maglev nanopositioning system as a case study. A National Instruments (NI) PXI-8110 real-time controller is used with two FPGAs (NI PXI-7854R and 7831R) to provide the necessary input/output (I/O) functions. Two Trust TA320 and two TA115 linear current amplifiers are utilized to power up the eight-phase coils. The sampling frequency is 5 kHz, and the current

TABLE I
OVERVIEW OF THE CONTROLLER PARAMETERS FOR Y AND X AXIS

Parameters	Y Axis		X Axis	
	Before Optimization	After Optimization	Before Optimization	After Optimization
K_p	30	25.1221	30	23.1781
T_i	0.002	2.8459×10^{-4}	0.002	3.8538×10^{-4}
T_d	0.00012	1.3490×10^{-4}	0.00012	2.3865×10^{-4}

TABLE II
OVERVIEW OF THE COST FUNCTIONS FOR Y AND X AXIS

Cost functions	Y Axis		X Axis	
	Before Optimization	After Optimization	Before Optimization	After Optimization
Total cost J	1.3892×10^8	2.4833×10^7	2.8850×10^6	6.1624×10^5
Tracking cost J_e	1.0890×10^8	5.6159×10^6	2.3326×10^6	3.9377×10^5
Control variation cost $J_{\dot{u}}$	3.0017×10^7	1.9217×10^7	5.5240×10^5	2.2247×10^5

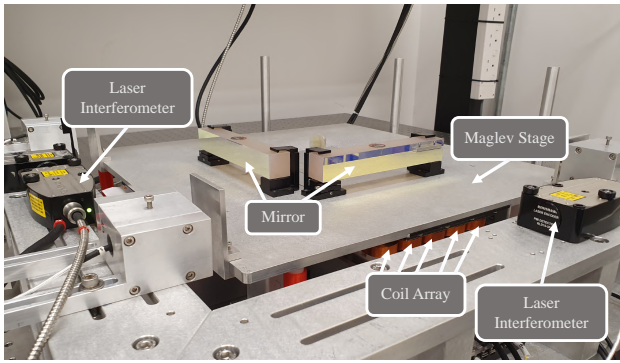


Fig. 4. Magnetically-levitated nanopositioning system used in the experimental validation.

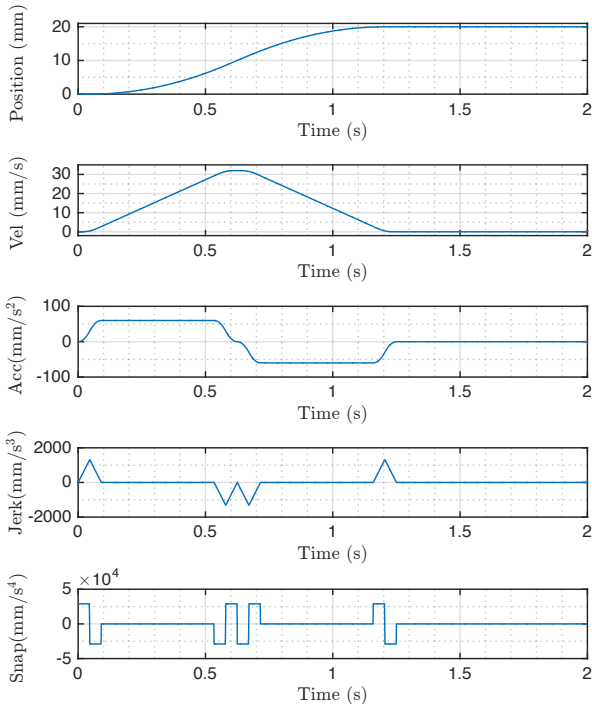


Fig. 5. Fourth-order S-curve motion profile used in the real-time experiment.

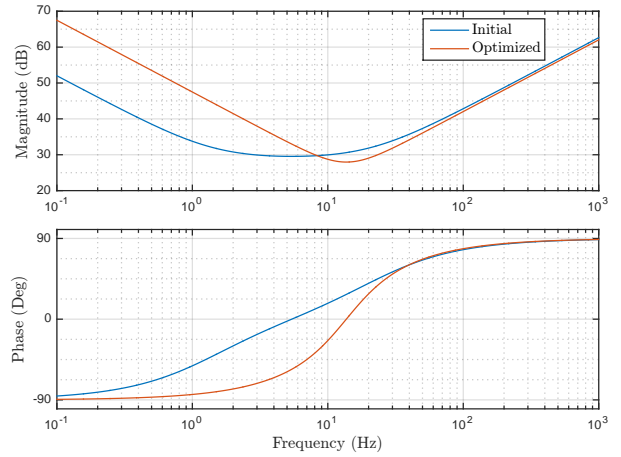


Fig. 6. Y axis controller $C(s, \rho)$ comparison before and after the optimization in the frequency domain.

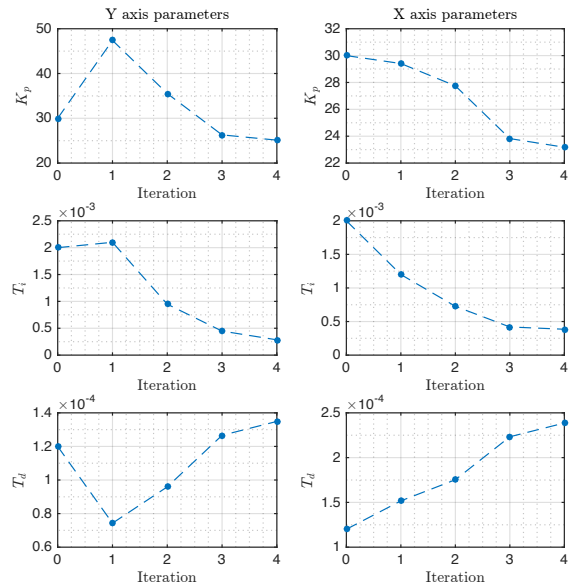


Fig. 7. Y axis and X axis controller parameter convergence diagram.

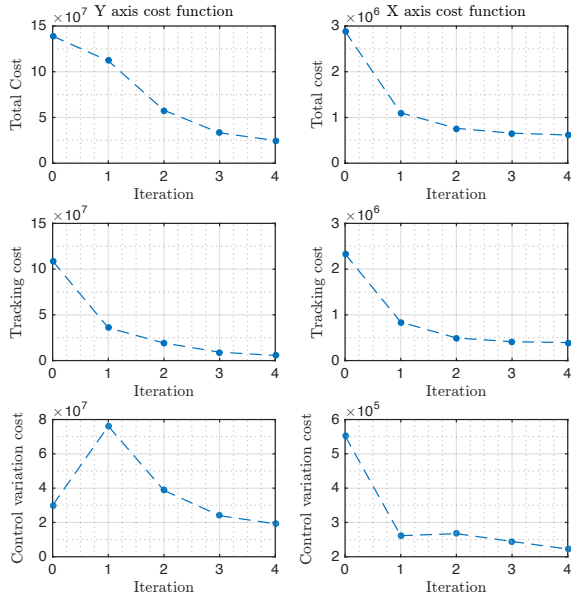


Fig. 8. Y axis and X axis cost function convergence diagram. Top: Overall Cost. Middle: Cost related to tracking error. Bottom: Cost related to control signal variation

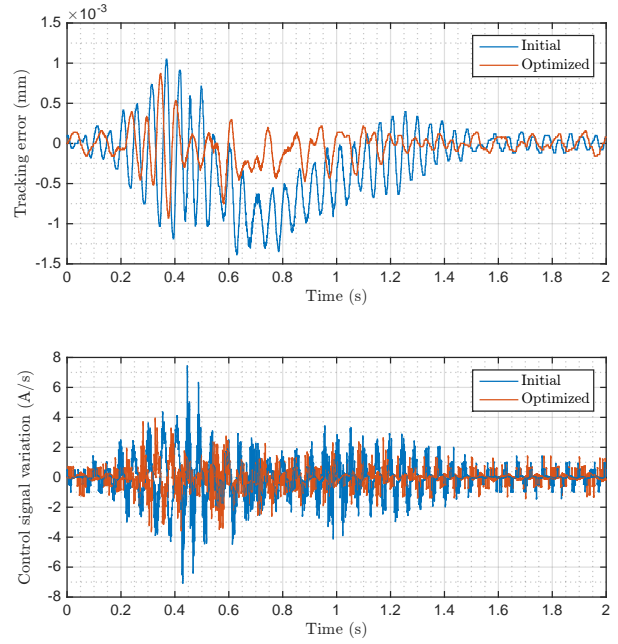


Fig. 10. X axis tracking error and control signal variation comparison before and after the data-driven multi-objective optimization.

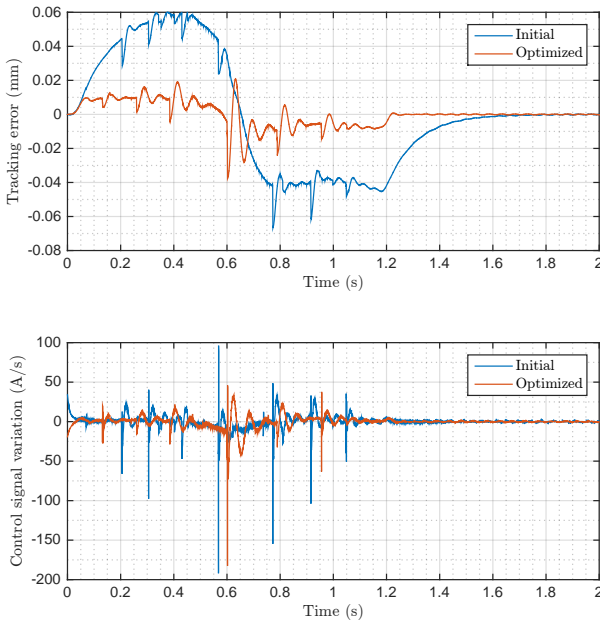


Fig. 9. Y axis tracking error and control signal variation comparison before and after the data-driven multi-objective optimization.

limit for each phase of the coil arrays is set as 1.2 A. The Renishaw fiber optic laser interferometers (Model: RLU10) are used for sensing of horizontal positions with a count resolution of 40 nm, and Lion Precision capacitive sensors (Model: CPL290 controller with C18 heads) are used for sensing of vertical positions with a root mean square resolution of 150 nm. The magnetically-levitated system including its actuation and sensor system are shown in Fig. 4, and its designed working range is 30 mm \times 30 mm \times 3 mm according to the coil array length.

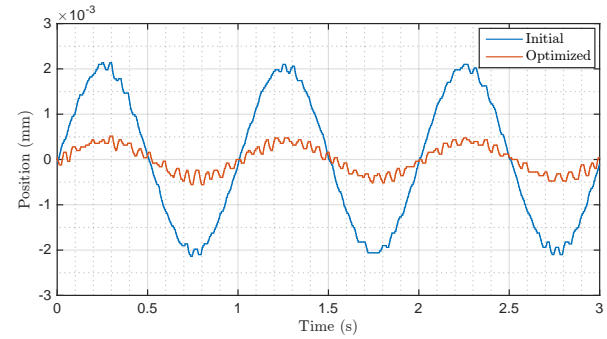


Fig. 11. X axis disturbance rejection performance comparison under 1 Hz sinusoidal disturbance.

The motion profile used in the experiment is a fourth-order S-curve which is particularly suitable for precision motion control [46]. In order to meet the requirement of smooth motion, the profile is defined up to the fourth order with limited jerk and snap. The position trajectory as well as its velocity, acceleration, jerk (time derivative of acceleration) and snap (time derivative of jerk) are plotted in Fig. 5. The magnetically-levitated system is controlled by a feedback controller in LabVIEW designed according to the typical proportionalintegralderivative (PID) structure, as the PID control is essentially the most widely adopted control structure in the industry. Nevertheless, it is pertinent at this juncture to also point out that the data-driven multi-objective optimization algorithm proposed here is also applicable to other types of feedback controllers, as long as that it can be expressed in the rather common and standard form of (7). Here specifically, the

control input $u(t)$ is

$$u(t) = K_p(e(t) + \frac{1}{T_i} \int_0^t e(t')dt' + T_d \frac{de(t)}{dt}), \quad (30)$$

and the feedback controller can be written in the form of (7) as

$$C(s, \rho) = \rho^T \bar{C}(s) = [K_p \quad K_p/T_i \quad K_p T_d] \begin{bmatrix} 1 \\ 1/s \\ s \end{bmatrix}. \quad (31)$$

The goal of the data-driven optimization is to find out the controller parameters that provide a smooth and accurate tracking of the motion profile in Fig. 5, i.e., minimizing the cost function $J(\rho)$ in (6). Note that during the optimization process, no *a priori* dynamic model information is needed nor will the algorithm attempt to build a model through system identification. To start with, the initial set of controller parameters ${}^0\rho$ is designed based on the loop shaping method in [47] with a second order model (neglecting the nonlinearities and higher order dynamics) and further fine-tuned to provide a decent but non-optimized control performance, as in Table I. It is worth noting, however, that loop shaping is a model-based method one can choose to use for the controller initialization but it is by no means necessary when there are no models available. In such cases, one shall simply tune the controller manually to achieve a decent performance and then rely on the proposed data-driven algorithm for performance optimization. The weightings are set as $w_1 = 10^7$ and $w_2 = 1$ so that the cost function values for the tracking error and control signal variation are on the same scale (the tracking error has a much smaller numerical value compared with the control signal variation). Nevertheless, we can still adjust the weightings according to the requirement of the motion system, i.e., further improvement on the accuracy or motion smoothness.

Despite the fact that the magnetically-levitated system is capable of conducting 6-DOF motion, we consider here only the X-Y plane motion because it is most commonly used in semiconductor manufacturing [48], [49]. Yet nevertheless, even in this application scenario, it is still the situation where the fully floating behavior and multi-axis coupling make extremely accurate identification of the motion dynamics largely impossible, so that traditional model-based approaches would encounter great difficulties in being properly successfully deployed here. In high precision semiconductor manufacturing applications, it is often required to conduct a series of repetitive motions [50], [51] on one of the axes. Meanwhile, in order to guarantee the accuracy of highly complex semiconductor circuit patterns, the tracking error from both Y and X axes needs to be minimized. Also, smooth motion should be ensured by minimizing the control input variation for both axes and using a higher-order S-curve trajectory. By using the proposed data-driven multi-objective optimization in **Algorithm 1**, the control parameters in both Y and X axes are iteratively optimized as shown in Table I and the control performance in terms of the cost function can be significantly improved as shown in Table II. In addition, a comparison of the optimized controller with the initial controller in the frequency domain is plotted in Fig. 6. One major advantage of

this data-driven approach is its fast convergence rate because it takes into account not only the gradient $\nabla J(i\rho)$ of the cost function but the Hessian $\nabla^2 J(i\rho)$. From Fig. 7 and Fig. 8, we can observe that both the controller parameters and cost function value converge within only four iterations. Note that the tracking cost J_e or control variation cost $J_{\dot{u}}$ alone may increase in some iteration, e.g., $J_{\dot{u}}$ of the Y axis in the 1st iteration, but the total cost J always decreases iteration by iteration. The time-domain performance improvement for Y axis before and after the data-driven optimization is plotted in Fig. 9, showing a significant reduction in both the tracking error and control signal variation; the root-mean-square (RMS) tracking errors are respectively 0.033 mm and 0.0075 mm. Here, the tracking error peaks, e.g., at 0.2 s of the initial result, could be due to the laser interferometer signal loss or computational delays. Meanwhile, the tracking error and control signal variation of the X axis are also reduced as shown in Fig. 10. The RMS tracking errors for X axis are respectively 4.8297×10^{-4} mm and 2.0365×10^{-4} mm. Here, the tracking error is much smaller compared with the Y axis, because the X axis is kept stationary while the Y axis is moving. After 1.5 s, the vibration still exists and this is due to the fact the stage is fully floating with little damping and has to deal with the disturbances from the force coupling. To further demonstrate the disturbance rejection performance, Fig. 11 shows the X axis position measurement comparison under the effect of a 1 Hz sinusoidal disturbance. From all these experimental results, we can see that the proposed approach is certainly effective and able to provide the appropriate optimized trajectory tracking in terms of both accuracy and smoothness, and the convergence rate is also suitably fast enough (only 4 iterations in our experiment) for practical applicability.

V. CONCLUSION

In this paper, we present a data-driven multi-objective optimization algorithm for repetitive motion tasks, where no *a priori* model information is available. The proposed algorithm is applied to a multi-axis magnetically-levitated system which is difficult to model accurately due to its fully floating behavior and multi-axis coupling. By making use of the rich information contained in the actual motion data under, say, the prevailing non-optimal conditions, the algorithm can provide fast, efficient and effective controller optimization for the system to operate towards optimality in a data-driven and iterative manner. A well-designed cost function is stated and specified, which takes both smooth and accurate tracking into account and the optimization process can be completed within a few iterations. Our experimental results show that the motion performance of the maglev nanopositioning system is enhanced significantly and could certainly meet the stringent requirement of present-day high-performance precision motion applications.

For future work, we believe applications of the proposed algorithm certainly is not be limited to such a multi-axis magnetically-levitated system only, and its potential can be further exploited and deployed in other robotic systems (es-

sentially especially those that are challenging to accurately model, e.g. quadrotors, legged robots, and soft robots, etc.).

REFERENCES

- [1] H. Zhu, T. J. Teo, and C. K. Pang, "Magnetically levitated parallel actuated dual-stage (maglev-pad) system for six-axis precision positioning," *IEEE/ASME Transactions on Mechatronics*, vol. 24, no. 4, pp. 1829–1838, Aug 2019.
- [2] V. H. Nguyen and W. Kim, "Two-phase lorentz coils and linear halbach array for multiaxis precision-positioning stages with magnetic levitation," *IEEE/ASME Transactions on Mechatronics*, vol. 22, no. 6, pp. 2662–2672, Dec 2017.
- [3] S. Kang, M. G. Lee, and Y. Choi, "Six degrees-of-freedom direct-driven nanopositioning stage using crab-leg flexures," *IEEE/ASME Transactions on Mechatronics*, vol. 25, no. 2, pp. 513–525, 2020.
- [4] S. Lu, C. Tian, and P. Yan, "Adaptive extended state observer-based synergetic control for a long-stroke compliant microstage with stress stiffening," *IEEE/ASME Transactions on Mechatronics*, vol. 25, no. 1, pp. 259–270, 2020.
- [5] S. Chen, H. Chiang, T. Liu, and C. Chang, "Precision motion control of permanent magnet linear synchronous motors using adaptive fuzzy fractional-order sliding-mode control," *IEEE/ASME Transactions on Mechatronics*, vol. 24, no. 2, pp. 741–752, 2019.
- [6] Y. Fan and U. Tan, "Design of a feedforward-feedback controller for a piezoelectric-driven mechanism to achieve high-frequency nonperiodic motion tracking," *IEEE/ASME Transactions on Mechatronics*, vol. 24, no. 2, pp. 853–862, 2019.
- [7] J. P. Mishra, Q. Xu, X. Yu, and M. Jalili, "Precision position tracking for piezoelectric-driven motion system using continuous third-order sliding mode control," *IEEE/ASME Transactions on Mechatronics*, vol. 23, no. 4, pp. 1521–1531, 2018.
- [8] Z. Wen, Y. Ding, P. Liu, and H. Ding, "An efficient identification method for dynamic systems with coupled hysteresis and linear dynamics: Application to piezoelectric-actuated nanopositioning stages," *IEEE/ASME Transactions on Mechatronics*, vol. 24, no. 1, pp. 326–337, 2019.
- [9] Q. Xu, "Continuous integral terminal third-order sliding mode motion control for piezoelectric nanopositioning system," *IEEE/ASME Transactions on Mechatronics*, vol. 22, no. 4, pp. 1828–1838, 2017.
- [10] K.-M. Lee, L. Li, K. Bai, X. Ouyang, and H. Yang, "Harmonic model and remedy strategy of multiphase pm motor under open-circuit fault," *IEEE/ASME Transactions on Mechatronics*, 2019.
- [11] Z. Wang, C. Hu, and Y. Zhu, "Dynamical model based contouring error position-loop feedforward control for multi-axis motion systems," *IEEE Transactions on Industrial Informatics*, 2019.
- [12] Z. Hou, H. Gao, and F. L. Lewis, "Data-driven control and learning systems," *IEEE Transactions on Industrial Electronics*, vol. 64, no. 5, pp. 4070–4075, 2017.
- [13] S. Yin, X. Li, H. Gao, and O. Kaynak, "Data-based techniques focused on modern industry: an overview," *IEEE Transactions on Industrial Electronics*, vol. 62, no. 1, pp. 657–667, 2015.
- [14] J. Ma, X. Li, and K. K. Tan, *Advanced Optimization for Motion Control Systems*. CRC Press, 2020.
- [15] C. Chen, S. Rai, and T. Tsao, "Iterative learning of dynamic inverse filters for feedforward tracking control," *IEEE/ASME Transactions on Mechatronics*, vol. 25, no. 1, pp. 349–359, 2020.
- [16] R. de Rozario, A. J. Fleming, and T. Oomen, "Finite-time learning control using frequency response data with application to a nanopositioning stage," *IEEE/ASME Transactions on Mechatronics*, 2019.
- [17] Y. Xie, X. Tang, W. Meng, B. Ye, B. Song, J. Tao, and S. Q. Xie, "Iterative data-driven fractional model reference control of industrial robot for repetitive precise speed-tracking," *IEEE/ASME Transactions on Mechatronics*, 2019.
- [18] W. Meng, S. Q. Xie, Q. Liu, C. Z. Lu, and Q. Ai, "Robust iterative feedback tuning control of a compliant rehabilitation robot for repetitive ankle training," *IEEE/ASME Transactions on Mechatronics*, vol. 22, no. 1, pp. 173–184, 2017.
- [19] J. Hwangbo, J. Lee, A. Dosovitskiy, D. Bellicoso, V. Tsounis, V. Koltun, and M. Hutter, "Learning agile and dynamic motor skills for legged robots," *Science Robotics*, vol. 4, no. 26, p. eaau5872, 2019.
- [20] Q. Li, J. Qian, Z. Zhu, X. Bao, M. K. Helwa, and A. P. Schoellig, "Deep neural networks for improved, impromptu trajectory tracking of quadrotors," in *2017 IEEE International Conference on Robotics and Automation (ICRA)*. IEEE, 2017, pp. 5183–5189.
- [21] M. C. Yip and D. B. Camarillo, "Model-less feedback control of continuum manipulators in constrained environments," *IEEE Transactions on Robotics*, vol. 30, no. 4, pp. 880–889, 2014.
- [22] —, "Model-less hybrid position/force control: a minimalist approach for continuum manipulators in unknown, constrained environments," *IEEE Robotics and Automation Letters*, vol. 1, no. 2, pp. 844–851, 2016.
- [23] L. Blanken, F. Boeren, D. Bruijnen, and T. Oomen, "Batch-to-batch rational feedforward control: from iterative learning to identification approaches, with application to a wafer stage," *IEEE/ASME Transactions on Mechatronics*, vol. 22, no. 2, pp. 826–837, 2016.
- [24] Q. Zhu, F. Song, J. Xu, and Y. Liu, "An internal model based iterative learning control for wafer scanner systems," *IEEE/ASME Transactions on Mechatronics*, 2019.
- [25] O. Koç, G. Maeda, and J. Peters, "Optimizing the execution of dynamic robot movements with learning control," *IEEE Transactions on Robotics*, vol. 35, no. 4, pp. 909–924, 2019.
- [26] F. Angelini, C. Della Santina, M. Garabini, M. Bianchi, G. M. Gasparri, G. Grioli, M. G. Catalano, and A. Bicchi, "Decentralized trajectory tracking control for soft robots interacting with the environment," *IEEE Transactions on Robotics*, vol. 34, no. 4, pp. 924–935, 2018.
- [27] Z. Q. Tang, H. L. Heung, K. Y. Tong, and Z. Li, "Model-based online learning and adaptive control for a human-wearable soft robot integrated system," *The International Journal of Robotics Research*. [Online]. Available: <https://doi.org/10.1177/0278364919873379>
- [28] C. Wang, M. Zheng, Z. Wang, and M. Tomizuka, "Robust two-degree-of-freedom iterative learning control for flexibility compensation of industrial robot manipulators," in *2016 IEEE International Conference on Robotics and Automation (ICRA)*. IEEE, 2016, pp. 2381–2386.
- [29] F. Berkenkamp, A. P. Schoellig, and A. Krause, "Safe controller optimization for quadrotors with Gaussian processes," in *2016 IEEE International Conference on Robotics and Automation (ICRA)*. IEEE, 2016, pp. 491–496.
- [30] H. Hjalmarsson, "Iterative feedback tuning-an overview," *International Journal of Adaptive Control and Signal Processing*, vol. 16, no. 5, pp. 373–395, 2002.
- [31] Y. Xie, J. Jin, X. Tang, B. Ye, and J. Tao, "Robust cascade path-tracking control of networked industrial robot using constrained iterative feedback tuning," *IEEE Access*, vol. 7, pp. 8470–8482, 2019.
- [32] M. Li, Y. Zhu, K. Yang, L. Yang, C. Hu, and H. Mu, "Convergence rate oriented iterative feedback tuning with application to an ultraprecision wafer stage," *IEEE Transactions on Industrial Electronics*, vol. 66, no. 3, pp. 1993–2003, 2019.
- [33] M. F. Heertjes, B. Van der Velden, and T. Oomen, "Constrained iterative feedback tuning for robust control of a wafer stage system," *IEEE Transactions on Control Systems Technology*, vol. 24, no. 1, pp. 56–66, 2016.
- [34] D. Son and H. Choi, "Iterative feedback tuning of the proportional-integral-differential control of flow over a circular cylinder," *IEEE Transactions on Control Systems Technology*, 2018.
- [35] M. Li, C. Mao, Y. Zhu, K. Yang, and X. Li, "Data-based iterative dynamic decoupling control for precision mimo motion systems," *IEEE Transactions on Industrial Informatics*, 2019.
- [36] X. Li, S.-L. Chen, C. S. Teo, and K. K. Tan, "Enhanced sensitivity shaping by data-based tuning of disturbance observer with non-binomial filter," *ISA transactions*, vol. 85, pp. 284–292, 2019.
- [37] H. Stearns, S. Mishra, and M. Tomizuka, "Iterative tuning of feedforward controller with force ripple compensation for wafer stage," in *2008 10th IEEE International Workshop on Advanced Motion Control*. IEEE, 2008, pp. 234–239.
- [38] S. H. van der Meulen, R. L. Tousain, and O. H. Bosgra, "Fixed structure feedforward controller design exploiting iterative trials: Application to a wafer stage and a desktop printer," *Journal of Dynamic Systems, Measurement, and Control*, vol. 130, no. 5, p. 051006, 2008.
- [39] X. Li, S.-L. Chen, C. S. Teo, and K. K. Tan, "Data-based tuning of reduced-order inverse model in both disturbance observer and feedforward with application to tray indexing," *IEEE Transactions on Industrial Electronics*, vol. 64, no. 7, pp. 5492–5501, 2017.
- [40] X. Li, S.-L. Chen, J. Ma, C. S. Teo, and K. K. Tan, "Data-driven model-free iterative tuning approach for smooth and accurate tracking," in *2018 IEEE/ASME International Conference on Advanced Intelligent Mechatronics (AIM)*. IEEE, 2018, pp. 593–598.
- [41] J. Ma, S.-L. Chen, C. S. Teo, A. Tay, A. Al Mamun, and K. K. Tan, "Parameter space optimization towards integrated mechatronic design for uncertain systems with generalized feedback constraints," *Automatica*, vol. 105, pp. 149–158, 2019.
- [42] J. Ma, X. Li, W. Liang, and K. K. Tan, "Parameter space optimization towards constrained controller design with application to tray indexing,"

IEEE Transactions on Industrial Electronics, vol. 67, no. 7, pp. 5575–5585, 2020.

- [43] H. Zhu, T. J. Teo, and C. K. Pang, “Design and modeling of a six-degree-of-freedom magnetically levitated positioner using square coils and 1-d halbach arrays,” *IEEE Transactions on Industrial Electronics*, vol. 64, no. 1, pp. 440–450, 2016.
- [44] S. Boyd and L. Vandenberghe, *Convex optimization*. Cambridge university press, 2004.
- [45] H. Hjalmarsson and S. Veres, “Robust loopshaping using iterative feedback tuning,” in *2001 European control conference (ECC)*. IEEE, 2001, pp. 2046–2051.
- [46] P. Lambrechts, M. Boerlage, and M. Steinbuch, “Trajectory planning and feedforward design for electromechanical motion systems,” *Control Engineering Practice*, vol. 13, no. 2, pp. 145–157, 2005.
- [47] H. Zhu, C. K. Pang, and T. J. Teo, “Analysis and control of a 6 DOF maglev positioning system with characteristics of end-effects and eddy current damping,” *Mechatronics*, vol. 47, pp. 183–194, 2017.
- [48] M. Yuan, Z. Chen, B. Yao, and X. Zhu, “Time optimal contouring control of industrial biaxial gantry: A highly efficient analytical solution of trajectory planning,” *IEEE/ASME Transactions on Mechatronics*, vol. 22, no. 1, pp. 247–257, 2016.
- [49] J. Ma, S.-L. Chen, N. Kamaldin, C. S. Teo, A. Tay, A. Al Mamun, and K. K. Tan, “Integrated mechatronic design in the flexure-linked dual-drive gantry by constrained linear–quadratic optimization,” *IEEE Transactions on Industrial Electronics*, vol. 65, no. 3, pp. 2408–2418, 2017.
- [50] K. K. Tan, X. Li, S.-L. Chen, C. S. Teo, and T. H. Lee, “Disturbance compensation by reference profile alteration with application to tray indexing,” *IEEE Transactions on Industrial Electronics*, vol. 66, no. 12, pp. 9406–9416, 2019.
- [51] X. Li, Q.-G. Wang, X. Li, K. K. Tan, and L. Xie, “Feedforward control with disturbance prediction for linear discrete-time systems,” *IEEE Transactions on Control Systems Technology*, vol. 27, no. 6, pp. 2340–2350, 2018.



Xiaocong Li (S'14–M'17) received the B.Eng. degree from the Department of Electrical and Computer Engineering, National University of Singapore, in 2013, and the Ph.D. degree in electrical engineering from the NUS Graduate School for Integrative Sciences and Engineering, National University of Singapore, in 2017.

He is a Research Scientist with the Mechatronics Group, Singapore Institute of Manufacturing Technology (SIMTech), Agency for Science, Technology and Research (A*STAR), where he is currently

leading a Collaborative Research Project (CRP) with the National University of Singapore on data-driven controls. Since 2018, he has served as a member of the Thesis Advisory Committee for NUS Graduate School for Integrative Science and Engineering. His current research interest is focused on making sense of data for controls through learning as well as its applications to robotics and precision motion systems.



Haiyue Zhu (S'13–M'17) received the B.Eng. degree in automation from the School of Electrical Engineering and Automation and the B. Mgt. degree in business administration from the College of Management and Economics, Tianjin University, Tianjin, China, in 2010, and the M.Sc. and Ph.D. degrees from the National University of Singapore (NUS), Singapore, in 2013 and 2017, respectively, both in electrical engineering.

He is currently a Scientist in Singapore Institute of Manufacturing Technology (SIMTech), Agency for

Science, Technology and Research (A*STAR). His current research interests include intelligent mechatronic and robotic systems, etc.



Jun Ma (S'15–M'18) received the B.Eng. degree with First Class Honours in electrical and electronic engineering from the Nanyang Technological University, Singapore, in 2014, and the Ph.D. degree in electrical and computer engineering from the National University of Singapore, Singapore, in 2018.

From 2018 to 2019, he was a Research Fellow with the Department of Electrical and Computer Engineering, National University of Singapore, Singapore. In 2019, he was a Research Associate with the Department of Electronic and Electrical Engineering, University College London, London, U.K. He is currently a Visiting Scholar with the Department of Mechanical Engineering, University of California, Berkeley, Berkeley, CA, USA. His research interests include control and optimization, precision mechatronics, robotics, and medical technology.

He was a recipient of the Singapore Commonwealth Fellowship in Innovation.



Tat Joo Teo (M'08) received the B. Eng. degree in mechatronics engineering from Queensland University of Technology, Australia, in 2003 and the Ph.D. degree from Nanyang Technological University, Singapore, in 2009.

He was a research scientist with the Singapore Institute of Manufacturing Technology, Singapore, from 2009 to 2018. He was a visiting scientist with Massachusetts Institute of Technology, USA, in 2016, and also served on the engineering faculty at the National University of Singapore and Newcastle

University in Singapore. His research interest is to explore the fundamentals of Newtonian mechanics, solid mechanics, kinematics, and electromagnetism to develop high precision mechatronics or robotic systems for micro-/nano-scale manipulation and bio-medical applications.

Dr. Teo has published over 50 peer-reviewed articles and has 4 patents granted. In 2013, he received the IECON Best Paper Award in the theory and servo design category. In 2014, he became the first Singaporean to win the R&D 100 Award, which is the most prestigious international award for technologically-significant products.



Chek Sing Teo (S'04–M'08) completed his Ph.D. degree at the National University of Singapore in 2008, under the Agency for Science Technology and Research (A-STAR) Scholarship Scheme, working on “Accuracy Enhancement for High Precision Gantry Stage”. His research interests are in the application of advanced control techniques to precision mechatronic system and instrumentation; to enhance performance in motion control and measurement. His current work includes using mechatronics stiffness to reduce jerk reaction in high speed motion

stage and sensor placement for adaptronics. He is currently working in the Singapore Institute of Manufacturing Technology (SIMTech) leading the Precision Mechatronics Team within the Mechatronics Group, as well as the co-Director of the SIMTech-NUS Precision Motion System joint lab.



Masayoshi Tomizuka (M'86-SM'95-F'97-LF'17) received the B.S. the and M.S. degrees in mechanical engineering from the Keio University, Tokyo, Japan, and the Ph.D. degree in mechanical engineering from the Massachusetts Institute of Technology in February 1974.

In 1974, he joined the faculty of the Department of Mechanical Engineering at the University of California at Berkeley, where he currently holds the Cheryl and John Neerhout, Jr., Distinguished Professorship Chair. His current research interests are optimal and

adaptive control, digital control, motion control, and their applications to robotics and vehicles.

He served as Program Director of the Dynamic Systems and Control Program of the Civil and Mechanical Systems Division of NSF (2002-2004). He served as Technical Editor of the ASME Journal of Dynamic Systems, Measurement and Control, J-DSMC (1988-93) and Editor-in-Chief of the IEEE/ASME Transactions on Mechatronics (1997-99). He is a Life Fellow of the ASME and IEEE, and a Fellow of International Federation of Automatic Control (IFAC) and the Society of Manufacturing Engineers. He is the recipient of the ASME/DSCD Outstanding Investigator Award (1996), the Charles Russ Richards Memorial Award (ASME, 1997), the Rufus Oldenburger Medal (ASME, 2002), the John R. Ragazzini Award (2006), and the Richard Bellman Control Heritage Award (2018).



Tong Heng Lee received the B.A. degree with First Class Honours in the Engineering Tripos from the Cambridge University, Cambridge, U.K., in 1980, the M.Engng. degree from the National University of Singapore (NUS), Singapore, in 1985, and the Ph.D. degree from the Yale University, New Haven, CT, USA, in 1987.

He is a Professor in the Department of Electrical and Computer Engineering at the National University of Singapore, and also a Professor in the NUS Graduate School, NUS NGS. He was a Past Vice-

President (Research) of NUS. Dr. Lee's research interests are in the areas of adaptive systems, knowledge-based control, intelligent mechatronics, and computational intelligence.

He currently holds Associate Editor appointments in the IEEE Transactions in Systems, Man and Cybernetics, Control Engineering Practice (an IFAC journal), and the International Journal of Systems Science (Taylor and Francis, London). In addition, he is the Deputy Editor-in-Chief of IFAC Mechatronics journal.